EFFECT OF CURVATURES IN THE BUCKLING ANALYSIS OF PERFORATED PLATES USING THE BOUNDARY ELEMENT METHOD

ROMILDO APARECIDO SOARES JUNIOR[1], VITOR CAUÊ GOMES[1],
LEANDRO PALERMO JUNIOR[1] & LUIZ CARLOS WROBEL[2]
[1]School of Civil Engineering, Architecture and Urban Design, State University of Campinas, Brazil
[2]Department of Civil Engineering, Pontifical Catholic University of Rio de Janeiro, Brazil

ABSTRACT
The buckling of perforated plates considering the effect of shear deformation is analyzed with the boundary element method. The geometrical non-linearity (GNL) effect included rotation derivatives (curvatures) as well as the deflection derivatives. The importance of the shear deformation in the buckling of perforated plates appeared with the increase of the plate thickness and the effect of curvatures becomes greater in large hole diameter cases.
Keywords: perforated plate buckling, Mindlin plate, Reissner plate, full non-linearity in buckling, critical loading.

1 INTRODUCTION

Plated structures are widely used in engineering and the in-plane forces result from the structural equilibrium to the external loads. Buckling analyses are usually employed in the design of plate elements of those structures. The inclusion of the effect of shear deformation in the bending model improves the accuracy of stress computation around holes [1], the plate behavior representation under dynamic condition [2] and the assessment of the critical buckling load changes according to the plate thickness as shown in the literature.

The inclusion of the rotation derivatives (curvatures) in the geometrical non-linearity effect (GNL) beyond the deflection derivatives is discussed in several studies on buckling analyses of thick plates considering the effect of shear deformation. Most studies on thick plate buckling only employed the deflection derivatives in the GNL as usually done in the well-known buckling analysis using the classical bending model [3]. Sun [4] presented a consistent study on the importance of curvatures in the buckling analyses with the effect of shear deformation. Trefftz and Biot theories were considered in Sun [4] and the effect of curvatures in buckling analyses became significant in the range of intermediate wavelengths, which corresponds to problems when the shear deformation is pronounced. An extensive study carried out by Mizusawa [5] showed the effect of curvatures can be significant or not, according to the type of the boundary conditions. Results obtained with the boundary element method (BEM) for buckling analyses including the effect of shear deformation and only the deflection derivatives in the GNL [6] agreed to those in the literature for square and rectangular plates with the thickness to plate side ratio in the range from 0.001 to 0.2. Buckling analyses with BEM including the curvatures (rotation derivatives) as well as the deflection derivatives in the GNL [7] confirmed the importance of curvatures according to the type of boundary conditions as pointed out by Mizusawa [5].

Levy et al. [8] studied the instability of reinforced perforated plates with a central hole under a uniform compression force. Brown and Yettram [9] studied how the value of the buckling parameter for different load combinations changes according to the hole diameter and the plate side ratio. Shakerley and Brown [10] studied plate buckling with eccentrically positioned holes. El-Sawy and Nazmy [11] used the finite element method to assess the

WIT Transactions on Engineering Sciences, Vol 134, © 2022 WIT Press
www.witpress.com, ISSN 1743-3533 (on-line)
doi:10.2495/BE450131

buckling parameter value for uniaxial loaded plates with different ratios between the hole diameter and the plate side. Jayashankarbabu and Karisiddappa [12] considered the buckling of perforated plates with the effect of shear deformation.

The studies on plate buckling in Soares and Palermo [6] and Palermo et al. [7] showed an efficient and light way to perform those analyses with the BEM. The eigenvalue analysis employing the inverse iteration with the Rayleigh quotient combined with the BEM solution, i.e., solution for values on the boundary followed by the solution for values in the domain, allowed a reduction in the order of the "matrices of the problem" and quick computation of required values in the domain as well as the final solution. Those features encouraged buckling analyses for other problems and the buckling of square and rectangular perforated plates were studied here with the effect of shear deformation with the GNL, including derivatives of deflections and rotations. An algebraic manipulation with the divergence theorem was done in the integral related to the GNL [7], which allowed to employ only the gradient of displacements in the non-linear analysis as well as to disregard the relation between derivatives of in-plane forces. Two integrals related to GNL resulted from this algebraic manipulation, with one computed in the domain and the other computed on the boundary, which is related to the natural conditions to perform the buckling analysis. The existence of holes required the plane stress problem solution at the beginning of the analysis to obtain the in-plane forces distribution in the domain. Quadratic shape functions approximated displacements (deflections and rotations), and tractions (distributed shears and moments) in the BEM whereas constant elements were used to discretize both integrals related to the GNL effect. The changes in the value of the buckling parameter according to the plate thickness and the hole diameter were compared to show the effect of the curvatures in the buckling analysis.

2 BOUNDARY INTEGRAL EQUATIONS

Isotropic plates were considered with the constitutive equations written next.

$$M_{\alpha\beta} = D\frac{(1-\nu)}{2}\left(u_{\alpha,\beta} + u_{\beta,\alpha} + \frac{2\nu}{1-\nu}u_{\gamma,\gamma}\delta_{\alpha\beta}\right), \tag{1}$$

$$Q_{\alpha} = D\frac{(1-\nu)}{2}\lambda^2\left(u_{\alpha} + u_{3,\alpha}\right), \tag{2}$$

with

$$D = \frac{Eh^3}{12(1-\nu^2)}; \quad \lambda^2 = 12\frac{\kappa^2}{h^2},$$

where u_α is the plate rotation in direction α, u_3 is the plate deflection, D is the flexural rigidity, h is the plate thickness, ν is Poisson's ratio, $\delta_{\alpha\beta}$ is the Kronecker delta. The Latin indices take on values {1, 2 and 3} and Greek indices take on values {1, 2}. The shear parameter is equal to 5/6 and $\pi^2/12$ for the Reissner and the Mindlin models, respectively, and it is the difference introduced in the analysis according to the model adopted.

The general form of the displacement boundary integral equations (DBIEs) with an additional domain integral containing the GNL effect is written next with Weeën's notation:

$$\frac{1}{2}C_{ij}(x')u_j(x') + \int_\Gamma \left[T_{ij}(x',x)u_j(x) - U_{ij}(x',x)t_j(x)\right]d\Gamma(x) = \cdots,$$

$$= \iint_\Omega \left\{U_{i3}(x',X)\left[\frac{\partial}{\partial X_\alpha}\left(N_{\alpha\beta}\frac{\partial u_3}{\partial X_\beta}\right)\right] + U_{i\gamma}(x',X)\frac{h^2}{12}\left[\frac{\partial}{\partial X_\alpha}\left(N_{\alpha\beta}\frac{\partial u_\gamma}{\partial X_\beta}\right)\right]\right\}d\Omega(X), \tag{3}$$

in which C_{ij} is an element of the matrix C related to the boundary at the source point, which becomes the identity matrix when a smooth boundary is considered, U_{ij} represents the rotation (j = 1, 2) or the deflection (j = 3) due to a unit couple (i = 1, 2) or a unit point force (I = 3), respectively, T_{ij} represents the moment (j = 1, 2) or the shear (j = 3) due to a unit couple (i = 1, 2) or a unit point force (i = 3), respectively.

The domain integral related to the GNL is converted into two integrals with the divergence theorem [7], with one computed on the boundary and the other in the domain. The gradient of displacements (rotations and deflection) becomes only necessary in the analysis, instead of second derivatives and no relation is required in the derivatives of in-plane forces. The final DBIE is given by:

$$\frac{1}{2}C_{ij}(x')u_j(x') + \int_\Gamma \left[T_{ij}(x',x)u_j(x) - U_{ij}(x',x)t_j(x)\right]d\Gamma(x) = \cdots$$

$$= \int_\Gamma \left[U_{i3}(x',x)n_\alpha(x)N_{\alpha\beta}(x)u_{3,\beta}(x) + \frac{h^2}{12}U_{i\gamma}(x',x)n_\alpha(x)N_{\alpha\beta}(x)u_{\gamma,\beta}(x)\right]d\Gamma(x) + \cdots$$

$$- \iint_\Omega \left[U_{i3,\alpha}(x',X)N_{\alpha\beta}(X)u_{3,\beta}(X) + \frac{h^2}{12}U_{i\gamma,\alpha}(x',X)N_{\alpha\beta}(X)u_{\gamma,\beta}(X)\right]d\Omega(X). \tag{4}$$

The boundary integral in eqn (4) can be related to the natural conditions, which can be obtained with the calculus of variations [7]. The natural conditions introduce requirements on the boundary portion with not prescribed displacements where the variations on displacements are not null ($\delta u_i \neq 0$). The natural conditions are given by:

$$t_\gamma = -\frac{h^2}{12}\left(n_\alpha N_{\alpha\beta}u_{\gamma,\beta}\right), \tag{5}$$

$$t_3 = -n_\alpha N_{\alpha\beta}u_{3,\beta}. \tag{6}$$

The tractions in eqns (5) and (6) are the boundary conditions introduced in eqn (4) when rotations and/or deflections are unknown in a part of the boundary edge. The boundary integral along the boundary portion with not prescribed displacements containing the natural conditions has the opposite signal of the boundary integral related to GNL in eqn (4) and it was considered in the numerical implementation.

The BIE for gradient of displacements is used in conjunction with eqn (4) in the buckling analysis. The BIE for the gradient of displacements at an internal point is next written in terms of differentiation of the field point coordinates and using the tangential differential operator [7], [13]:

$$u_{i,\gamma}(X') = \int_\Gamma \left\{M_{i\alpha\beta}(X',x)D_{\gamma\alpha}\left[u_\beta(x)\right] + n_\gamma(x)Q_{i\beta}(X',x)u_\beta(x)\right\}d\Gamma(x) + \cdots$$

$$+ \int_\Gamma \left\{Q_{i\beta}(X',x)D_{\gamma\beta}[u_3(x)] - U_{ij,\gamma}(X',x)t_j(x)\right\}d\Gamma(x) + \cdots$$

$$+\int_{\Gamma}\left[U_{i3,\gamma}(x',x)n_{\alpha}(x)N_{\alpha\beta}(x)u_{3,\beta}(x)+\frac{h^2}{12}U_{i\rho,\gamma}(x',x)n_{\alpha}(x)N_{\alpha\beta}(x)u_{\rho,\beta}(x)\right]d\Gamma(x)+$$

$$-\iint_{\Omega}\left[U_{i3,\alpha\gamma}(x',X)N_{\alpha\beta}(X)u_{3,\beta}(X)+\frac{h^2}{12}U_{i\rho,\alpha\gamma}(x',X)N_{\alpha\beta}(X)u_{\rho,\beta}(X)\right]d\Omega(X), \qquad (7)$$

with,

$$D_{\alpha\beta}[f(x)]=n_{\alpha}(x)f_{,\beta}(x)-n_{\beta}(x)f_{,\alpha}(x).$$

The solution of the generalized plane stress problem is required to obtain the in-plane force distribution on the domain of perforated plates at the beginning of the buckling analyses. The BIEs for plane stress problems are given by:

$$\frac{1}{2}C_{\alpha\beta}(x')v_{\beta}(x')+\int_{\Gamma}P_{\alpha\beta}(x',x)v_{\beta}(x)d\Gamma(x)=\int_{\Gamma}V_{\alpha\beta}(x',x)p_{\beta}(x)d\Gamma(x), \qquad (8)$$

$$N_{\alpha\gamma}(X')=S_{\alpha\gamma\kappa\theta}\int_{\Gamma}\sigma_{\kappa\delta\beta}(X',x)D_{\theta\delta}\left[v_{\beta}(x)\right]d\Gamma-\int_{\Gamma}\sigma_{\beta\alpha\gamma}(X',x)p_{\beta}(x)d\Gamma, \qquad (9)$$

where v_β and p_β are the in-plane displacements and tractions in direction β of the plane stress problem, respectively. $V_{\alpha\beta}$ and $P_{\alpha\beta}$ represent the displacement and traction in direction β due to a unit force in direction α, respectively.

The BIE for stresses at internal points, eqn (9), was written in terms of differentiation of the field point coordinates, the Hooke tensor for isotropic media ($S_{\alpha\gamma\kappa\theta}$) and using the tangential differential operator $D_{\theta\delta}$. The transversal modulus (G) in the Hooke tensor was multiplied by the plate thickness to use $N_{\alpha\gamma}$ in eqns (4) and (7).

3 THE NUMERICAL IMPLEMENTATION

The numerical implementation is the same used in Soares and Palermo [6] and Palermo et al. [7], with quadratic shape functions for isoparametric boundary elements. The nodes are always placed at ends in case of continuous or discontinuous elements. The collocation points were placed at nodes in case of continuous elements or shifted inside the element at positions ±0.67, in the range (–1, 1), respectively to the end where the discontinuity exists. Singularity subtraction [14] and the transformation of variable technique [15] were employed for the Cauchy and the weak type of singularity, respectively, when integrations were performed on elements containing the collocation points. The standard Gauss–Legendre scheme was employed for integrations of elements (or side of the cell) not containing the collocation points. The GNL effect was introduced using integrations on constant rectangular cells in the domain [6], [7]. The derivatives of the displacements (deflection and rotation) at the center of the cell were assumed constant on each cell, which allowed the use of the divergence theorem to convert the domain integral into equivalent boundary integrals performed on sides of the cell. This strategy allowed to compute the GNL effect using integrations on sides of cells inside the domain in all problems. Additional integrations were performed on sides of cells along the plate edge only when the natural conditions required, i.e.:

(a) When the displacements are prescribed on the whole boundary (a clamped plate on all sides), no integrations related to the GNL effect were computed on sides of cells along the plate edges. No natural condition was required.

(b) When the displacements are not prescribed on the boundary portion of the plate (free edge), integrations related to the GNL were computed on sides of cells along the free edge.
(c) In the case of the hard or the soft boundary condition, when the deflection is prescribed and the rotation in the normal direction or both rotations is/are not prescribed, integrations related to the curvature in the GNL effect corresponding to the rotation released were computed on sides of cells along the plate.

The in-plane stress distribution according to in-plane boundary conditions of the perforated plates was obtained at the beginning of the problem with eqns (8) and (9). The values obtained for in-plane stresses at the center of cells are used in the discretized form of eqns (4) and (6). The eigenvalue analysis [6, 7. 16] used the basic inverse iteration and the Rayleigh quotient. The iteration procedure continued until the absolute difference between values of successive eigenvalues was less than 10^{-8}.

4 NUMERICAL EXAMPLES

The Young modulus (E) was 206.9 GPa, the Poisson ratio (ν) was 0.3. The Mindlin model was employed. The buckling parameter k is a non-dimensional value related to the critical load of the plate (N_{cr}), the length of the plate side (a) and the flexural rigidity (D), which is obtained according to following expression:

$$k = \frac{a^2 N_{cr}}{\pi^2 D}.$$

Three cases shown in Fig. 1 were studied: (a) Square plate with a hole at the center, (b) Rectangular plate with a hole near one of the ends, and (c) Rectangular plate with a hole near the center. The plates were uniformly compressed with free longitudinal edges for in-plane boundary conditions. The plates were simply supported for the buckling problem and

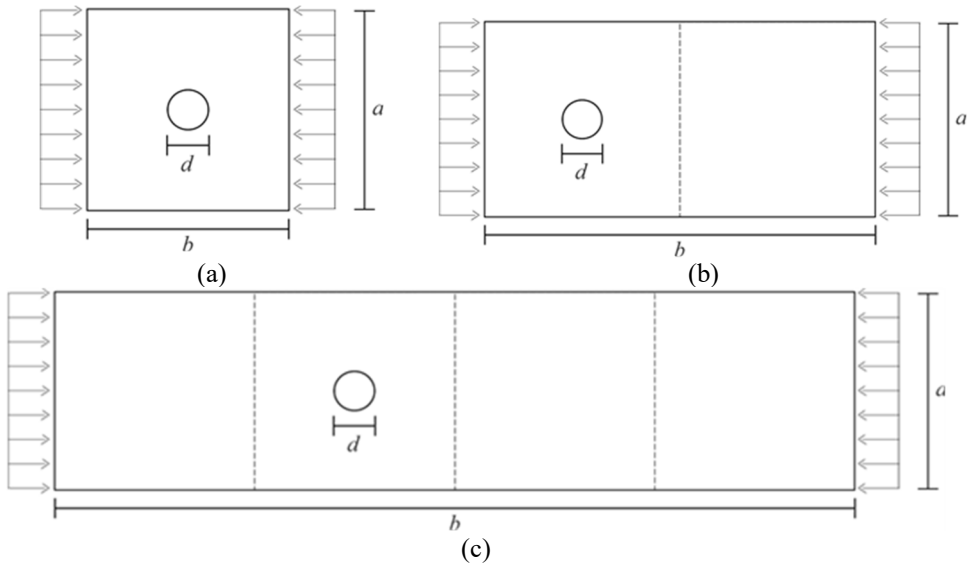

Figure 1: Studied plates. (a) Square plate; (b) Rectangular plate (b = 2a); and (c) Rectangular plate (b = 4a).

the hard restraint condition (twist moments restrained) used in all external sides. The free edge condition was used along the boundary of the hole.

The adopted meshes are presented in Table 1 and the results obtained are plotted in Figs 2 to 4, whereas the correspond buckling values are presented in Tables 2 to 4. Results obtained in Soares and Palermo [6] for the square and the rectangular plate (b = 2a) without holes were included only for comparison purpose.

Table 1: Number of adopted boundary elements and domain cells.

Case	**Square plate**		**Rectangular plate (b = 2a)**		**Rectangular plate (b = 4a)**	
d/a	BE	Cells	BE	Cells	BE	Cells
0	128	256	192	512		
0.1	192	448	272	848	432	1648
0.2	208	460	288	860	448	1660
0.3	224	464	304	864	464	1664
0.4	240	460	320	860	480	1660
0.5	256	448	336	848	496	1648
0.6	272	428	352	828	512	1628
0.7	288	400	368	800	528	1600

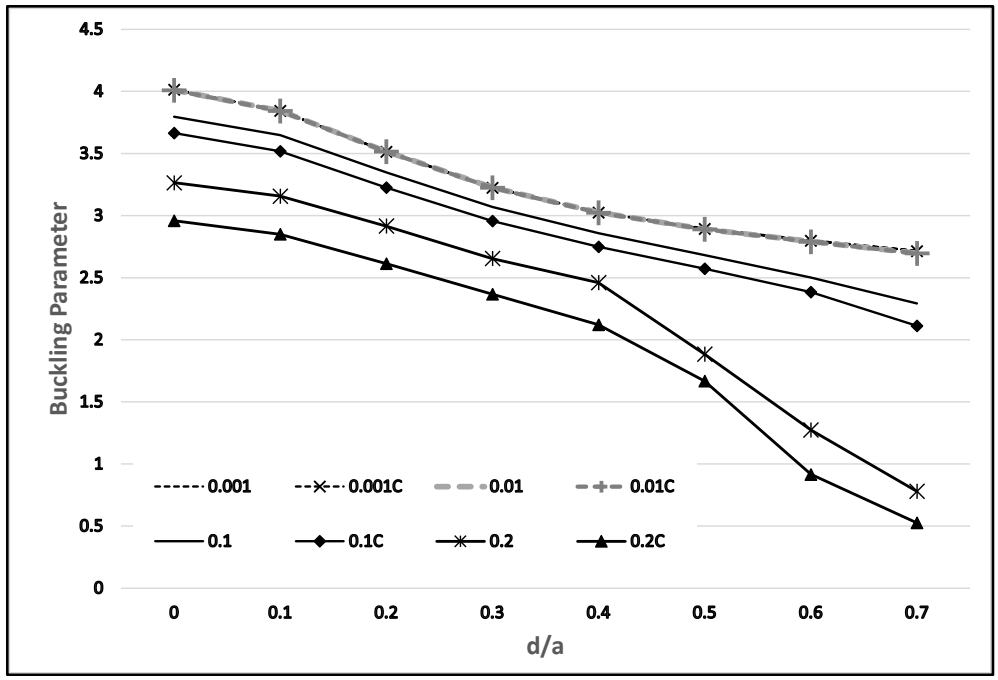

Figure 2: Results for the square plate.

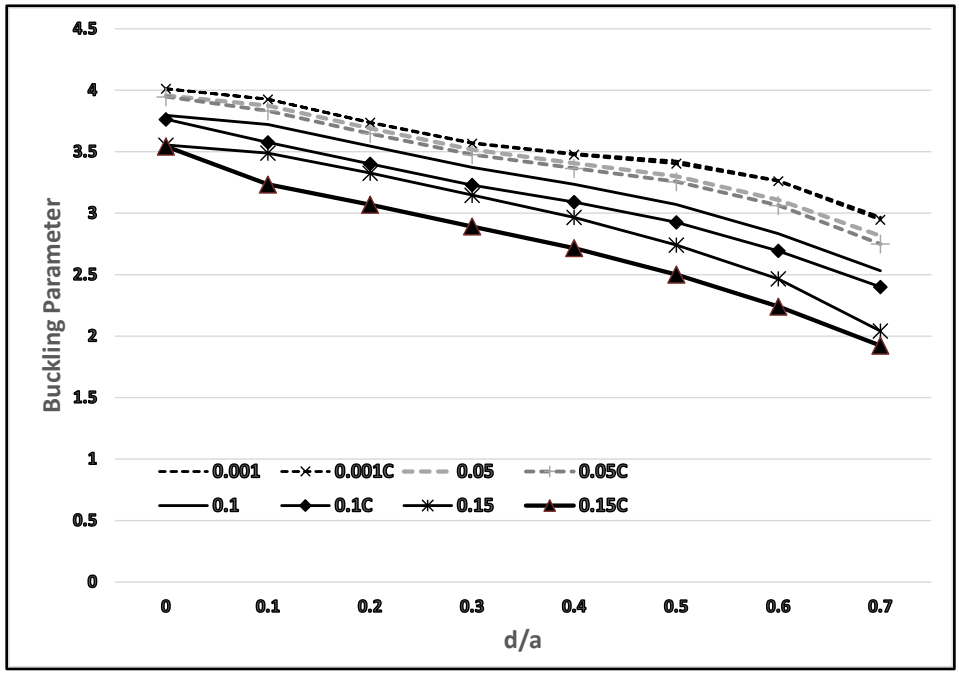

Figure 3: Results for the rectangular plate (b = 2a).

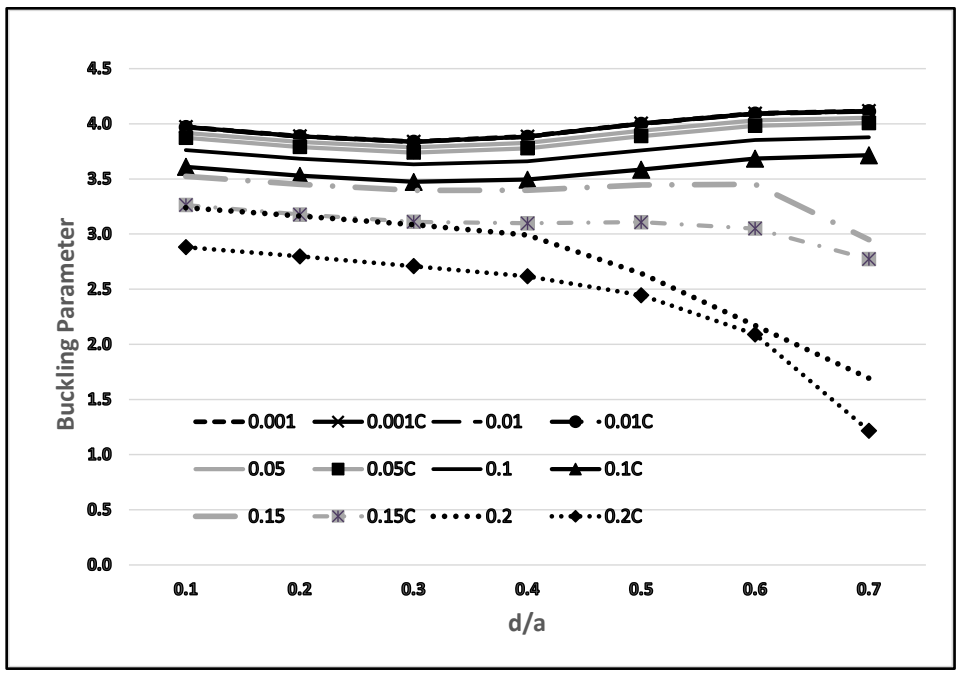

Figure 4: Results for the long rectangular plate (b = 4a).

Table 2: Values obtained for the square plate.

d/a	h/a							
	0.001	0.001C	0.01	0.01C	0.1	0.1C	0.2	0.2C
0	4.0128	4.0127	4.0105	4.0088	3.7952	3.6638	3.2643	2.9587
0.1	3.8437	3.8428	3.8442	3.8427	3.6471	3.5186	3.1559	2.8498
0.2	3.5165	3.5143	3.5166	3.5152	3.3481	3.2261	2.9152	2.6134
0.3	3.2269	3.2239	3.2260	3.2248	3.0706	2.9558	2.6545	2.3670
0.4	3.0269	3.0236	3.0244	3.0232	2.8578	2.7475	2.4601	2.1209
0.5	2.8959	2.8925	2.8904	2.8892	2.6829	2.5726	1.8840	1.6679
0.6	2.8008	2.7975	2.7900	2.7888	2.5005	2.3838	1.2738	0.9161
0.7	2.7165	2.7136	2.6972	2.6959	2.2929	2.1116	0.7799	0.5252

Table 3: Values obtained for the rectangular plate (b = 2a).

d/a	h/a							
	0.001	0.001C	0.05	0.05C	0.1	0.1C	0.15	0.15C
0	4.0127	4.0126	3.9561	3.9466	3.7952	3.7638	3.5543	3.5435
0.1	3.9275	3.9269	3.8746	3.8320	3.7205	3.5756	3.4889	3.2335
0.2	3.7394	3.7371	3.6895	3.6475	3.5457	3.4018	3.3261	3.0695
0.3	3.5724	3.5673	3.5176	3.4761	3.3723	3.2295	3.1465	2.8924
0.4	3.4850	3.4754	3.4074	3.3653	3.2342	3.0903	2.9664	2.7164
0.5	3.4227	3.4032	3.3001	3.2563	3.0713	2.9259	2.7415	2.5011
0.6	3.2653	3.2602	3.1079	3.0636	2.8350	2.6936	2.4658	2.2411
0.7	2.9668	2.9453	2.8149	2.7492	2.5315	2.4002	2.0420	1.9230

Table 4: Values obtained for the rectangular plate (b = 4a).

d/a	h/a									
	0.01	0.01C	0.05	0.05C	0.1	0.1C	0.15	0.15C	0.2	0.2C
0.1	3.9704	3.9686	3.9172	3.8725	3.7598	3.6089	3.5235	3.2628	3.2397	2.8808
0.2	3.8859	3.8842	3.8348	3.7895	3.6825	3.5282	3.4515	3.1776	3.1646	2.7979
0.3	3.8367	3.8351	3.7851	3.7386	3.6318	3.4725	3.3957	3.1113	3.0851	2.7089
0.4	3.8824	3.8807	3.8257	3.7774	3.6606	3.4940	3.3984	3.0974	2.9907	2.6165
0.5	4.0047	3.9981	3.9380	3.8883	3.7584	3.5836	3.4438	3.1079	2.6438	2.4455
0.6	4.0910	4.0890	4.0308	3.9824	3.8532	3.6839	3.4515	3.0493	2.1720	2.0904
0.7	4.1138	4.1118	4.0538	4.0062	3.8769	3.7153	2.9475	2.7729	1.6934	1.2169

All analyses considered six values for the thickness to plate side ratio: 0.001, 0.01, 0.05, 0.1, 0.15 and 0.2. The results obtained with deflection and rotation derivatives in the GNL were presented for each thickness with letter C included (Complete), whereas results obtained with only deflections derivatives in the GNL were presented without the letter C. The results obtained with thickness to plate side ratios 0.001, 0.01, 0.1 and 0.2 were plotted in Fig. 2 whereas those for ratios 0.001, 0.05, 0.1 and 0.15 were plotted in Fig. 3. This was done in different figures for a clearer visualization. Results obtained with ratio 0.001 were not included in Table 4 but they are plotted in Fig. 4.

The effect of the thickness increase and the curvatures were significant for h/a equal or greater than 0.1 in the square plate (Fig. 2). The reduction in the buckling parameter has a significant decrease with the increase of the diameter.

The effect of the thickness increase and the curvatures was significant for h/a equal or greater than 0.05 for the rectangular plate in Fig. 3. The reduction in the buckling parameter has a significant decrease with the increase of the diameter.

The effect of the thickness increase and the curvatures were significant for h/a equal to 0.2 for the long rectangular plate in Fig. 4. The reduction in the buckling parameter was not significant with the increase of the diameter for ratios until 0.10 and the reduction became significant when the effect of curvatures was included.

5 CONCLUSIONS

Results obtained for buckling analyses of perforated plates with the BEM has shown the importance of considering curvatures in the GNL effect. According to values plotted in Fig. 4, the plate buckling behavior can be incorrectly represented without the inclusion of the curvatures in the GNL effect. The use of the divergence theorem in the GNL effect results in disregard of a relation between stress derivatives and the GNL, and worked with the gradient of displacements. This formulation simplified some features in BEM formulations for buckling analyses employing second derivatives of displacements and requiring a relation between stress derivatives. The present formulation considering the tangential differential operator in the BIEs for the gradient of displacements or in the BIE for stresses carried to employ only Cauchy type singularities. Furthermore, the buckling formulation using BEM can be considered a light computational formulation due to the reduction of the order of the matrices related to the problem, which benefits the computational time for the solution.

ACKNOWLEDGEMENTS

The authors are grateful to CAPES and CNPq for the financial support in the development of this research.

REFERENCES

[1] Reissner, E., The effect of transverse shear deformation on the bending of elastic plates. *Journal of Applied Mechanics*, **12**(2), pp. A66–A77, 1945.

[2] Mindlin, R.D., Influence of rotatory inertia and shear on flexural motions of isotropic elastic plates. *Journal of Applied Mechanics*, **18**, pp. 18–31, 1951.

[3] Timoshenko, S.P. & Woinowsky-Krieger, S., *Theory of Plates and Shells*, 2nd ed., McGraw-Hill: New York, 1959.

[4] Sun, C.T., On the equations for a Timoshenko beam under initial stress. *J. Appl. Mech.*, **39**, pp. 282–285, 1972.

[5] Mizusawa, T., Buckling of rectangular Mindlin plates with tapered thickness by the spline strip method. *International Journal of Solids and Structures*, **30**(12), pp. 1663–1677, 1993.

[6] Soares Jr, R.A. & Palermo Jr, L., Effect of shear deformation on the buckling parameter of perforated and non-perforated plates studied using the boundary element method. *Engineering Analysis with Boundary Elements*, **85**, pp. 57–69, 2017.
[7] Palermo Jr, L., Gomes, V.C. & Wrobel, L.C., Plate buckling including effects of shear deformation and plate bending curvatures using the boundary element method, boundary elements and other mesh reduction methods XLIV. *WIT Transactions on Engineering Sciences*, vol. 131, WIT Press: Southampton and Boston, pp. 95–105, 2021.
[8] Levy, S., Woolley, R.M. & Kroll, W.D., Instability of simply supported square plate with reinforced circular hole in edge compression. *Journal of Research*, pp. 571–577, 1947.
[9] Brown, C.J. & Yettram, A.L., The elastic stability of square perforated plates under combinations of bending, shear, and direct load. *Thin-Walled Structures*, **4**(3), pp. 239–246, 1986.
[10] Shakerley, T.M. & Brown, C.J., Elastic buckling of plates with eccentrically positioned rectangular perforations. *International Journal of Mechanical Sciences*, **38**(8), pp. 825–838, 1996.
[11] El-Sawy, K.M. & Nazmy, A.S., Effect of aspect ratio on the elastic buckling of uniaxially loaded plates with eccentric holes. *Thin-Walled Structures*, **39**(12), pp. 983–998, 2001.
[12] Jayashankarbabu, B. & Karisiddappa, K., Stability of square plate with concentric cutout. *International Journal of Emerging Technology and Advanced Engineering*, **3**(8), pp. 259–267, 2013.
[13] Palermo Jr., L., The tangential differential operator applied to a stress boundary integral equation for plate bending including the shear deformation effect. *Eng. Anal. Bound. Elem*., **36**, pp. 1213–1225, 2012.
[14] Wrobel, L.C., *The Boundary Element Method: Applications in Thermo-Fluids and Acoustics*, John Wiley: Chichester, 2002.
[15] Telles, J.C.F., A self-adaptive coordinate transformation for efficient numerical evaluation of general boundary element integrals. *Int. J. Num. Meth. Eng*., **24**, pp. 959–973, 1987.
[16] Wilkinson, J.H., *The Algebraic Eigenvalue Problem*, Oxford University Press, William Clowes & Sons: London, 1972.